Wannier based analysis of the direct-indirect bandgap transition by stacking MoS_2 layers

Shunsuke Hirai, ¹ Ibuki Terada, ¹ and Michi-To Suzuki^{1, 2}

¹Department of Materials Science, Graduate School of Engineering,
Osaka Metropolitan University, Sakai, Osaka 599-8531, Japan

²Center for Spintronics Research Network, Graduate School of Engineering Science,
Osaka University, Toyonaka, Osaka 560-8531, Japan
(Dated: July 2025)

Molybdenum disulfide (MoS₂), a layered van der Waals material, has attracted considerable attention as a promising alternative to graphene for applications in field-effect transistors and nanophotonic devices because of its sizable band gap, high carrier mobility, large on/off ratio, and strong photoluminescence efficiency. A particularly intriguing property of MoS₂ is the transition of its band gap character with layer thickness: while the monolayer exhibits a direct gap, the band gap becomes indirect in multilayer and bulk forms. To clarify the microscopic mechanism behind this transition, we performed first-principles calculations combined with Wannier-based modeling, focusing on the roles of atomic orbitals and interlayer interactions. While orbitals oriented perpendicular to the plane—such as $\text{Mo-}d_{z^2}$ and $\text{S-}p_z$ —have been considered the primary contributors, our analysis reveals that in-plane p_x and p_y orbitals of S atoms also play a significant role. These findings highlight the importance of both out-of-plane and in-plane orbital contributions in governing the electronic structure of layered MoS₂, providing deeper insight into its band gap engineering for future device applications.

I. INTRODUCTION

Transition metal dichalcogenides (TMDs) have emerged as a fascinating class of materials owing to their layered structures and the diverse physical properties that arise from reduced dimensionality[1–3]. Because the inter layer bonding is relatively weak, dominated by van der Waals interactions, individual monolayers can be readily exfoliated, making TMDs ideal platforms for exploring novel two-dimensional phenomena. Their thin-film forms often exhibit electronic, optical, and mechanical properties that differ markedly from those of the bulk, which has spurred intensive interest in their potential applications in nanoelectronics or optoelectronics.

Among TMDs, molybdenum disulfide (MoS₂) has received particular attention due to its remarkable electronic properties [4, 5]. One of the most striking properties of MoS₂ is the change in bandgap character with layer thickness: bulk MoS₂ is an indirect-gap semiconductor, whereas monolayer MoS₂ exhibits a direct gap. This behavior was first predicted theoretically [6] and later confirmed experimentally through photoluminescence measurements [7–9]. These pioneering studies triggered extensive research efforts into the fundamental physics of monolayer MoS₂ and related TMDs.

From an application standpoint, the unique layer-dependent band structure of MoS₂ makes it a strong candidate for flexible semiconductors, optoelectronic devices, and field-effect transistors (FETs). In particular, its high carrier mobility and excellent on/off current ratio have made MoS₂-based FETs a central focus of device-oriented studies [10]. For such applications, understanding and controlling the evolution of the electronic structure with layer number is of crucial impor-

tance. In this work, we provide a detailed analysis of the microscopic mechanism behind the direct-to-indirect band gap transition in MoS₂ induced by layer increasing. Using first-principles calculations combined with Wannier-based modeling, we clarify the roles of specific atomic orbitals and interlayer interactions in shaping the electronic band structure. Our results not only deepen the fundamental understanding of layer-dependent band structure evolution but also provide insights into strategies for band gap engineering in van der Waals materials for future device applications.

II. CALCULATION DETAILS

The crystal structure of 2H-MoS₂ is shown in Fig. 1. The hexagonal unit cell contains two Mo atoms and four S atoms. Each Mo atom is coordinated by six S atoms in a trigonal prismatic arrangement, forming S–Mo–S layers stacked along the c-axis in an ABA sequence with weak van der Waals interactions between adjacent layers. The space group is P63/mmc with 2c sites, $(\frac{1}{3}, \frac{2}{3}, \frac{1}{4})$ and $(\frac{2}{3}, \frac{1}{3}, \frac{3}{4})$, for Mo and 4f sites, $(\frac{1}{3}, \frac{2}{3}, u)$ $(\frac{2}{3}, \frac{1}{3}, \bar{u})$ $(\frac{1}{3}, \frac{2}{3}, \frac{1}{2} - u)$ and $(\frac{2}{3}, \frac{1}{3}, \frac{1}{2} + u)$, for S. The experimentally determined lattice constants are a = 3.160 Å and c = 12.294 Å, and the internal parameter is u = 0.621 [11].

In this study, first-principles calculations were performed within Density Functional Theory (DFT) using generalized gradient approximation (GGA) with the PBE sol functional, implemented in QUANTUM ESPRESSO [13, 14]. The plane-wave cutoff was set to 150 Ry for the wavefunctions and 600 Ry for the charge density. For the bulk system, an $8\times8\times8$ Monkhorst–Pack k-point mesh was used for self consistent field (SCF) calculations

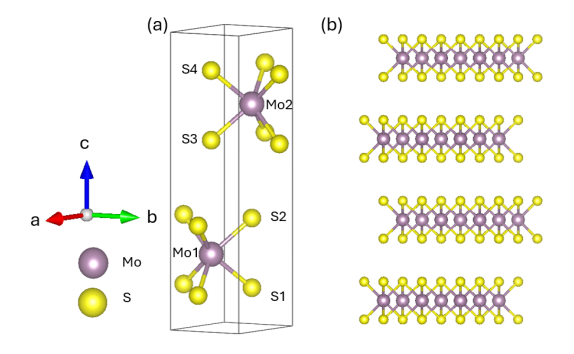


FIG. 1. Crystal structure of 2H-MoS₂: (a) unit cell and (b) side view of layer structure. This figure are drawn by VESTA[12].

and an $18 \times 18 \times 18$ mesh for the calculations of Density of States. The optimized lattice constants in bulk form were a=3.14 Å and c=12.6 Å, with the internal parameter determined as u=0.6259. For the monolayer system, a supercell approach was employed with a vacuum spacing of about 60 Å between periodic images. An $8\times 8\times 2$ k-point mesh was adopted for the monolayer supercell SCF calculation.

A Tight-binding model was constructed using Wannier90 [15] based on the bulk electronic structure calculated with Quantum ESPRESSO. In this study, following Ref. [16], we choose the Mo-4d and S-3p orbitals as projection orbitals, which primarily contribute to the electronic states near the Fermi level, as shown in Fig. 2. To obtain multi-layer electronic states, we constructed the Hamiltonian for an N-layer system using the bulk tight-binding (TB) model. The Hamiltonian is written as

$$\mathcal{H}_{N} = \sum_{l,l'=1}^{N} |l\rangle \,\mathcal{H}_{ll'} \,\langle l'| \,, \tag{1}$$

where $|l\rangle$ denotes the l-th layer basis state. The block Hamiltonian $\mathcal{H}_{ll'}$ corresponds to the intralayer interaction in the Hamiltonian when l=l', and to the interlayer interaction in the Hamiltonian when $l\neq l'$. Here, the matrix elements of $\mathcal{H}_{ll'}$ was obtained from the bulk TB model. We use open boundary conditions along the c-axis to describe the multi-layer system. The constructed Hamiltonian describes the N=2M layers system, where M denotes the number of unit cells stacked along the c-axis. In the monolayer calculation, we use only the block Hamiltonian of the bottom layer in the unit cell illustrated in Fig. 1(a).

III. RESULTS AND DISCUSSION

In this study, we investigated the mechanism behind the transition of the energy-gap structure of MoS₂ from a direct transition in the monolayer to an indirect transition in the multilayer structure based on first-principles

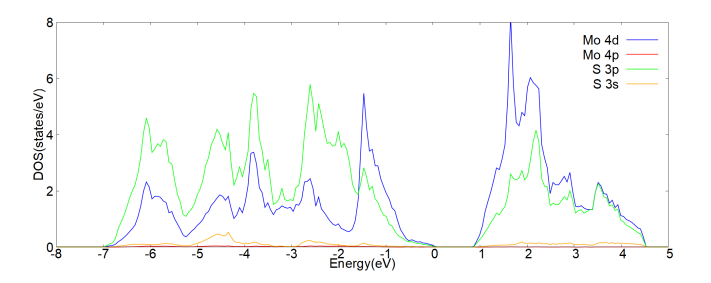


FIG. 2. Density of states of bulk MoS₂

calculations. To investigate in detail the relationship between the electronic states and atomic orbitals, we also constructed a TB model based on first-principles calculations as mentioned in section II.

Our TB model for bulk MoS₂ well reproduces the bands around the energy gap as shown in Fig. 3 (a). The band structure of monolayer and multilayer MoS₂ was obtained using the TB model described in the calculation details. The monolayer band structure of MoS₂ are shown in Fig. 3(b). The TB results showed good agreement with the DFT results and were demonstrated to be useful for multilayer calculations. In monolayer MoS₂, the transition point is the K point. In contrast, in the bulk, the transition points are the Γ point in the valence band and a point between the K point and the Γ point in the conduction band, $\mathbf{k} = (0.177, 0.177, 0)$, referred to as the Q point in this paper as shown in Fig. 3(c). This evolution is accompanied by a reduction of the band gap: 1.72 eV in the monolayer and 0.958 eV in the bulk. Our result is consistent with previous studies [6, 7, 17–19].

To examine how the band structure evolves with increasing number of layers, we calculated the band structures for monolayer, bilayer and 6-layer systems (Fig. 4). The stacked layers increase the energy bands and caused band splitting. Significant modifications in the overall band structure arise from noticeable band splittings appearing in certain regions of the Brillouin zone. The band splitting is small at K point indicated by the blue circles in Fig. 4 whereas the band splitting is large at the Qand Γ points indicated by the red circles. Consequently as the number of layers increases, the conduction-band bottom or valence-band top move from the points with small band splitting to those where the splitting is large. Specifically, the valence-band top shifts from the K point to the Γ point, while the conduction-band bottom shifts from the K point to the Q point. Therefore, understanding what causes the band splitting is crucial for elucidating the mechanism of changes in band structure. We discuss the band splitting from the perspective of atomic orbitals.

First, we focus on the relationship between band splitting and orbitals at valence band. Fig. 5 (a)-(d) shows the contributions for energy band from the Mo 4d orbitals and the S 3p orbitals, respectively. The Mo d_{z^2} orbital (58.5%) and S p_z orbital (41.2%) are dominant at the Γ point where the band splitting is large. In contrast,

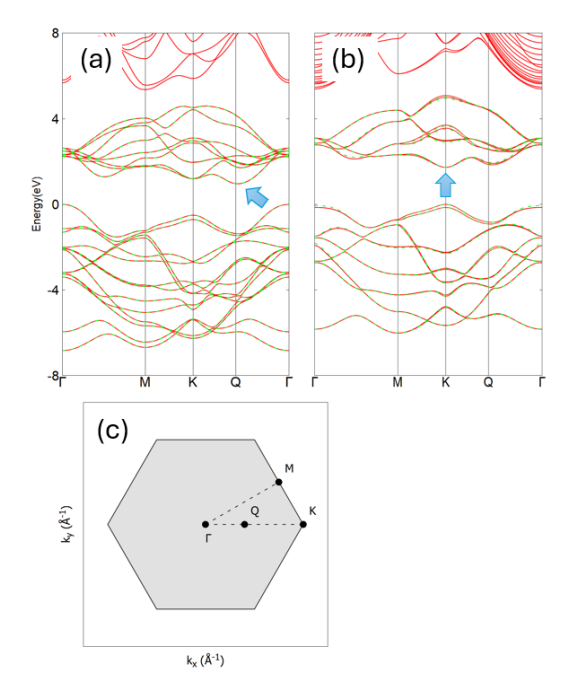


FIG. 3. Comparison of band structure by DFT(red solid lines) and TB model(green broken lines) : (a) bulk and (b) monolayer MoS_2 . The arrows indicate the band-gap transitions. (c) Brillouin Zone of MoS_2

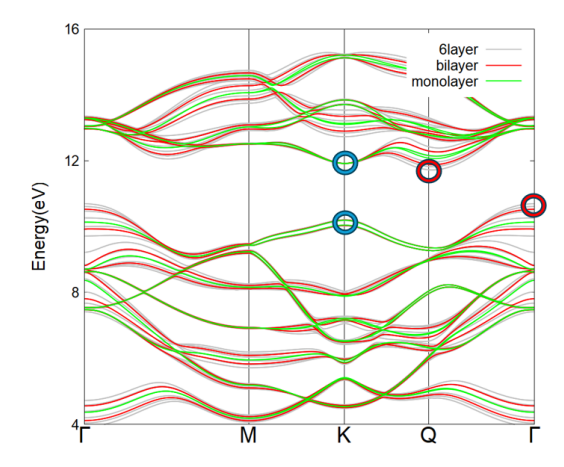


FIG. 4. Band structure for monolayer (green), bilayer (red), and 6-layers (gray) MoS₂.

Mo $d_{x^2-y^2}$ and d_{xy} orbitals (82.0%) and the S p_x and p_y orbitals (17.7%) are dominant at the K point where the band splitting is small. This result suggests that orbitals perpendicular to the layer exhibit significant band splitting of the valence band. We confirmed this trend between orbitals and band splitting from the perspective of the k-space Hamiltonian shown in TABLE I. We define the electronic state of atom A's orbital α at point k as $|A\alpha k\rangle$, where $\langle A\alpha k|H|B\beta k\rangle$ represents the magnitude of the interaction between the α orbital of atom A and the β orbital of atom B. At the Γ point, the Hamiltonian matrix elements describing the interaction

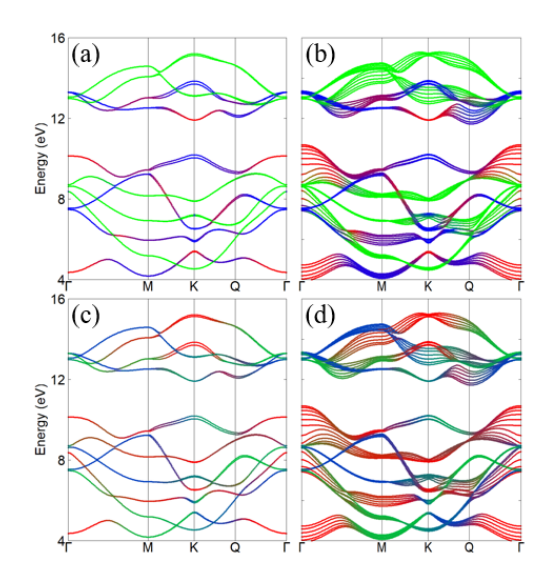


FIG. 5. (a)(b) The Mo d orbital character of the MoS₂ band structure for (a)monolayer and (b)6-layer. The orbital weights are represented as follows: d_{z^2} (red), d_{xz} and d_{yz} (green), and d_{xy} and $d_{x^2-y^2}$ (blue). (c)(d) The S p orbital character of the MoS₂ band structure for (c)monolayer and (d)6-layer. The orbital weights are represented as follows: p_z (red), p_x (green), and p_y (blue).

between S p_z orbitals or S p_z and Mo d_{z^2} orbitals across layers are significantly large among the matrix elements corresponding interlayer interaction in Hamiltonians. In contrast,interlayer interaction elements in Hamiltonians have a small absolute value at the K-point. These results provide quantitative confirmation that orbitals perpendicular to the layer exhibit strong interlayer interactions and significant band splitting as menthiond in the pervious work [6, 18].

Next, we discuss the conduction band. In the conduction band, the aforementioned trend does not appear to hold at first glance. The band splitting is small at the K point despite the large orbital weight of Mo d_{z^2} orbitals (82.6%), whereas it is large at the Q point despite the small orbital weight of S p_z (12.1%) and Mo d_{z^2} (10.7%) orbitals and large orbital weight of planer orbitals to the layer (73.9% in total) such as S p_x (9.0%), p_y (17.1%) and Mo $d_{x^2-y^2}$ (28.7%), d_{xy} (19.1%).

Since it is difficult to understand the trend of band splitting solely from the orbital weight for the conduction band, we examine the trend from the perspective of the k-space Hamiltonian (TABLE I). At K point with small band splitting, both Mo d_{z^2} and S p_z orbitals involved in interlayer interactions are small. This result suggests that the electronic states at the K point are dominated by intralayer interactions, which in turn result in a small band splitting when layers are stacked. At the Q point, the interlayer $p_z - p_z$, $p_z - p_x$ and $p_z - p_y$ interactions are particularly strong. This indicates that the S p_z orbital, in cooperation with the p_x and p_y orbital, causes significant band splitting due to strong interlayer

TABLE I. Matrix elements corresponding to the interlayer interaction in the Hamiltonian arranged in order of absolute value (eV) at each k-point.

Q point	absolute value	K point	absolute value	Γ point	absolute value
$\langle S_2 p_z Q H S_3 p_z Q \rangle$	0.696	$\langle S_2 p_x K H S_3 p_x K \rangle$	0.105	$\langle S_2 p_z \Gamma H S_3 p_z \Gamma \rangle$	0.932
$\langle S_2 p_z Q H S_3 p_y Q \rangle$	0.250	$\langle S_2 p_y K H S_3 p_y K \rangle$	0.104	$\langle \operatorname{Mo}_1 d_{z^2} \Gamma H \operatorname{S}_3 p_z \Gamma \rangle$	0.161
$\langle S_2 p_z Q H S_3 p_x Q \rangle$	0.159	$\langle S_2 p_x K H S_3 p_y K \rangle$	0.102	$\langle \mathrm{Mo}_1 d_{z^2} \Gamma H \mathrm{Mo}_2 d_{z^2} \Gamma \rangle$	0.072
$\langle \operatorname{Mo}_1 d_{x^2 - y^2} Q H \operatorname{S}_3 p_z Q \rangle$	0.100	$\left \left\langle \operatorname{Mo}_{1}d_{z^{2}}K\right H\left \operatorname{S}_{3}p_{z}K\right\rangle \right $	0.037	$\langle S_1 p_z \Gamma H S_3 p_z \Gamma \rangle$	0.046
$\langle S_2 p_x Q H S_3 p_x Q \rangle$	0.099	$\left \left\langle \operatorname{Mo}_{1} d_{xy} K \right H \left \operatorname{S}_{3} p_{x} K \right\rangle \right $	0.033	$\langle S_2 p_x \Gamma H S_3 p_x \Gamma \rangle$	0.043

interaction. This result is noteworthy, considering that the p_x and p_y orbital are in-plane orbitals. This suggests that the interlayer coupling involves not only the out-of-plane component but also in-plane contributions from the p_x and p_y orbitals. It is also noteworthy that a clear anisotropy is observed between the p_x and p_y orbitals. The Hamiltonian in TABLE I shows that the interaction between p_z and p_y orbitals is larger than that between p_z and p_x orbitals, and the contribution for orbital weight from the p_y orbital is also larger than that from the p_x orbital in Fig. 5.

We examined how strongly the interlayer interactions affect the band splitting by recalculating the band energies with specific interlayer couplings— p_z – p_z , p_z – p_x , and p_z - p_y -removed at the Q and Γ points. In these calculations, the Hamiltonian matrix elements corresponding interlayer interactions (for example, $\langle S_2 p_z Q | H | S_3 p_z Q \rangle$ for the p_z - p_z interaction at the Q point) were set to zero, and the band energies of the bulk were obtained without these interactions. As a result, the energy level at the valence band top at Γ point was lowered by 0.315 eV when the p_z - p_z interaction was removed. In contrast, the energy level remained unchanged when the p_z-p_x and p_z-p_y interactions were removed. These results can be explained by the dominant contribution of the p_z orbital and the relatively small contributions of the p_x and p_y orbitals at the valence band top at Γ point. At the conduction band bottom at Q point, removing the p_z - p_z interlayer interaction resulted in an energy increase of 0.079 eV, whereas removing the p_z-p_x and p_z-p_y interactions led to a 0.081 eV increase. These results indicate that the p_z - p_x and p_z - p_y interlayer interactions contribute to the band splitting almost as much as that of the p_z-p_z interaction at Q point. At both Q and Γ points, the magnitudes of the Hamiltonian matrix elements for orbitals shown in TA-BLE I is consistent with its effect on the band splitting.

The above results can be visually grasped from the k-resolved charge density ρ_{nk} which is defined by the following expression:

$$\rho_{n\mathbf{k}} = \phi_{n\mathbf{k}}^*(\mathbf{r})\phi_{n\mathbf{k}}(\mathbf{r}), \tag{2}$$

where n is band index, k is wave vector and $\phi_{nk}(r)$ is the Kohn–Sham wavefunction. This k-resolved charge density ρ_{nk} has the relationship with the conventional

charge density $\rho(\mathbf{r})$ as follows:

$$\rho(\mathbf{r}) = \sum_{n} \frac{1}{(2\pi)^3} \int d^3k \ \rho_{n\mathbf{k}}(\mathbf{r}). \tag{3}$$

We computed the k-resolved charge density ρ_{nk} using DFT, as shown in Fig. 6. Figures 6 (a) and (c) show the charge density at valence band top at Γ point and conduction band bottom at Q point, where exhibit significant band splitting. In both cases electrons are spread between the layers, indicating strong interlayer coupling. Figures (b) and (d) show the charge densities at the points of small band splitting at the valance band top and conduction band bottom at K point. In contrast to Figs. 6(a)(c) at the k-points indicating large band splitting, electrons are localized only within the layers with a small inter-layer distribution. These k-resolved charge densities reflect the correlation between the interlayer orbital interactions and the resulting band splitting discussed above.

In summary, our study concludes that interlayer interactions involving the sulfur p_z orbital, together with its hybridization with in-plane orbitals such as p_x and p_y , play a central role in determining the magnitude of the band splitting. Strong interlayer coupling mediated by the p_z orbital at the conduction-band at Q point and the valence-band at Γ point leads to large band splittings, whereas the much weaker p_z contributions at K point result in only minor splitting. This behavior reflects the fact that Hamiltonian matrix elements associated with the p_z orbital are particularly strong, owing to the broad out-of-plane extension of p_z -derived electronic states, which enhances their susceptibility to interlayer coupling. Our analysis further reveals that, although the p_z orbital provides the dominant contribution, in-plane orbitals $(p_x \text{ and } p_y)$ also contribute by forming interlayer couplings through hybridization with p_z .

IV. CONCLUSIONS

In this study, we investigated the origin of band structure changes in exfoliated MoS_2 from an atomic orbital perspective. Specifically, the orbital contributions to the band structure, the k-space Hamiltonian, and the k-resolved charge density were examined. This research demonstrated that S p_z orbitals are the dominant factor

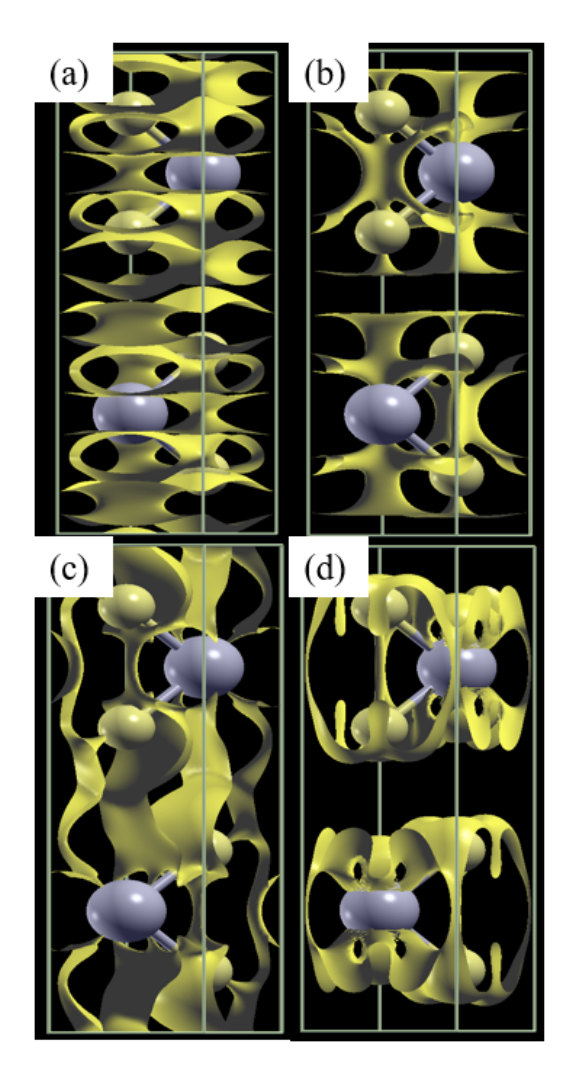


FIG. 6. The k-resolved charge density distribution for bulk MoS₂ at (a) Γ point in valence band top (b) K point in valence band top (c) Q point in conduction band bottom (d) K point in conduction band bottom. These figures are drawn by XCrysDen[20].

in driving the band structure changes while in-plane orbitals such as S p_x and p_y also play a meaningful role in band gap modification. The difference in the magnitude of band splitting due to layering induces changes in the band structure; in the valence (conduction) band, the transition point shifts from the K point to the Γ point (Q point). Our study show that the magnitude of the band splitting near the Fermi level is determined not by the Mo d_{z^2} orbital, but rather by the S p orbitals. The p_z-p_y interlayer interaction ranks second in importance to the $p_z - p_z$ interaction in contributing to the band splitting at Q point. These attributes can be quantitatively evaluated via the k-space TB Hamiltonian and also confirmed from the spatial distribution of the k-resolved charge density. Our results not only clarify the mechanism of the band splitting associated with the transition from a direct to an indirect band gap induced by the stacking of MoS₂ layers, but also suggest strategies for engineering its band structure through orbital and interlayer interaction control.

ACKNOWLEDGMENTS

We are grateful to K. Tanno for the technical supports. We also thank M. Ochi for helpful comments and discussions. This research is supported by JSPS KAKENHI Grants Numbers JP23H01130, JP24K00581, JP24K00588, JP25K00947, JP25K21684.

^[1] M. Chhowalla, Z. Liu, and H. Zhang, Chem. Soc. Rev. 44, 2584 (2015).

^[2] G.-B. Liu, D. Xiao, Y. Yao, X. Xu, and W. Yao, Chem. Soc. Rev. 44, 2643 (2015).

^[3] A. Kuc and T. Heine, Chem. Soc. Rev. 44, 2603 (2015).

^[4] X. Li and H. Zhu, J. Materiomics 1, 33 (2015).

O. V. Yazyev and A. Kis, Mater. Today 18, 20 (2015).

^[6] T. Li and G. Galli, J. Phys. Chem. C 111, 16192 (2007).

^[7] A. Splendiani, L. Sun, Y. Zhang, T. Li, J. Kim, C.-Y. Chim, G. Galli, and F. Wang, Nano Lett. 10, 1271 (2010).

^[8] K. F. Mak, C. Lee, J. Hone, J. Shan, and T. F. Heinz, Phys. Rev. Lett. 105, 136805 (2010).

^[9] G. Eda, H. Yamaguchi, D. Voiry, T. Fujita, M. Chen, and M. Chhowalla, Nano Letters 11, 5111 (2011).

^[10] B. Radisavljevic, A. Radenovic, J. Brivio, V. Giacometti, and A. Kis, Nat. Nanotechnol. 6, 147 (2011).

^[11] R. G. Dickinson and L. Pauling, J. Am. Chem. Soc. 45, 1466 (1923).

^[12] K. Momma and F. Izumi, J. Appl. Cryst. 44, 1272 (2011).

^[13] P. Giannozzi, O. Andreussi, T. Brumme, O. Bunau, M. Buongiorno Nardelli, M. Calandra, R. Car, C. Cavazzoni, D. Ceresoli, M. Cococcioni, N. Colonna, I. Carnimeo, A. Dal Corso, S. de Gironcoli, P. Delugas, R. A. DiStasio, A. Ferretti, A. Floris, G. Fratesi, G. Fugallo, R. Gebauer, U. Gerstmann, F. Giustino, T. Gorni, J. Jia, M. Kawamura, H.-Y. Ko, A. Kokalj, E. Küçükbenli, M. Lazzeri, M. Marsili, N. Marzari, F. Mauri, N. L. Nguyen, H.-V. Nguyen, A. Otero-de-la Roza, L. Paulatto, S. Poncé, D. Rocca, R. Sabatini, B. Santra, M. Schlipf, A. P. Seitsonen, A. Smogunov, I. Timrov, T. Thonhauser, P. Umari, N. Vast, X. Wu, and S. Baroni, J. Phys. Condens. Matter 29, 465901 (2017).

- [14] P. Giannozzi, S. Baroni, N. Bonini, M. Calandra, R. Car, C. Cavazzoni, D. Ceresoli, G. L. Chiarotti, M. Cococcioni, I. Dabo, A. Dal Corso, S. de Gironcoli, S. Fabris, G. Fratesi, R. Gebauer, U. Gerstmann, C. Gougoussis, A. Kokalj, M. Lazzeri, L. Martin-Samos, N. Marzari, F. Mauri, R. Mazzarello, S. Paolini, A. Pasquarello, L. Paulatto, C. Sbraccia, S. Scandolo, G. Sclauzero, A. P. Seitsonen, A. Smogunov, P. Umari, and R. M. Wentzcovitch, J. Phys. Condens. Matter 21, 395502 (2009).
- [15] G. Pizzi, V. Vitale, R. Arita, S. Blügel, F. Freimuth, G. Géranton, M. Gibertini, D. Gresch, C. Johnson, T. Koretsune, J. Ibañez-Azpiroz, H. Lee, J.-M. Lihm, D. Marchand, A. Marrazzo, Y. Mokrousov, J. I. Mustafa,
- Y. Nohara, Y. Nomura, L. Paulatto, S. Poncé, T. Ponweiser, J. Qiao, F. Thöle, S. S. Tsirkin, M. Wierzbowska, N. Marzari, D. Vanderbilt, I. Souza, A. A. Mostofi, and J. R. Yates, J. Phys. Condens. Matter **32**, 165902 (2020).
- [16] E. Ridolfi, D. Le, T. S. Rahman, E. R. Mucciolo, and C. H. Lewenkopf, J. Phys. Condens. Matter 27, 365501 (2015).
- [17] T. Cheiwchanchamnangij and W. R. Lambrecht, Phys. Rev. B 85, 205302 (2012).
- [18] E. S. Kadantsev and P. Hawrylak, Solid State Commun. 152, 909 (2012).
- [19] S. Ahmad and S. Mukherjee, Graphene 3, 52 (2014).
- [20] A. Kokalj, J. Mol. Graph. Model. 17, 176 (1999).